Available online at www.sciencedirect.com
ScienceDirect
Ceramics International 36 (2010) 491–496
CERAMICS INTERNATIONAL
www.elsevier.com/locate/ceramint

Properties of Si_3N_4–TiN composites fabricated by spark plasma sintering by using a mixture of Si_3N_4 and Ti powders

Norhayati Ahmad [a,b], Hidekazu Sueyoshi [a,*]

[a] Department of Nano-structure and Advanced Materials, Graduate School of Science and Engineering, Kagoshima University, 1-21-40 Korimoto, Kagoshima 890-0065, Japan
[b] Department of Materials Engineering, Faculty of Mechanical Engineering, Universiti Teknologi Malaysia, 81310 UTM Skudai, Johor, Malaysia

Received 11 June 2009; received in revised form 27 July 2009; accepted 2 September 2009
Available online 12 October 2009

Abstract

Si_3N_4–TiN composites were successfully fabricated via planetary ball milling of 70 mass% Si_3N_4 and 30 mass% Ti powders, followed by spark plasma sintering (SPS) at 1250–1350 °C. The sintering mechanism for SPS was a hybrid of dissolution–reprecipitation and viscous flow. The electrical resistivity decreased with increasing sintering temperature up to a minimum at 1250 °C and then increased with the increasing sintering temperature. The composites prepared by SPS at 1250–1350 °C could be easily machined by electrical discharge machining. Composite prepared by SPS at 1300 °C showed a high hardness (17.78 GPa) and a good machinability.

Keywords: C. Electrical conductivity; C. Mechanical properties; D. Si_3N_4; Spark plasma sintering

1. Introduction

Silicon nitride (Si_3N_4) based ceramics have been widely studied as candidates for technical and engineering applications due to their excellent mechanical properties and good corrosion and thermal shock resistance [1,2]. Recent years, various components have complex shapes and hence, require machining generally by diamond tools, which leads to high machining cost. Electrical discharge machining (EDM) is a potential and attractive technology for the machining of ceramics, provided that these materials have a sufficiently high electrical conductivity. A successful approach is to incorporate electrically conductive reinforcement to the insulating Si_3N_4 matrix such as TiN, TiB_2, ZrB_2 and TiC [3–5]. It is well known that TiN ceramic showing high electrical conductivity ($4.6 \times 10^6\ \Omega^{-1}\ m^{-1}$) has also been used to improve the fracture toughness of Si_3N_4 [6]. Furthermore, thermodynamic calculations indicate that TiN is compatible with Si_3N_4 [7]. Si_3N_4–TiN composites have been investigated in order to obtain a combination of high fracture toughness, high hardness and low electrical resistivity [8]. Si_3N_4–TiN composites can be synthesized by high energy milling of silicon nitride and titanium powder [9] or by coating nano-sized TiN particles on Si_3N_4 powders, which are prepared through a chemical route [10]. Other processing routes are conventional powder preparation route which are liquid phase sintering of Si_3N_4 and TiN powder mixtures [11] and CVD process using gas mixtures of $SiCl_4$–$TiCl_4$–NH_3–H_2 [12]. We have reported the preparation of Si_3N_4–TiN composites via planetary ball milling of Si_3N_4 and 20 vol% TiN powders [13]. The composites prepared by SPS at 1550 and 1600 °C had low electrical resistivity and could be machined by EDM. The in situ synthesis process which used Ti and Si_3N_4 powders enables the production of composites with the following advantages: low cost, reduce process step, desirable microstructures, provide fine scale reinforcement and enhanced sinterability. However, there are limited reports of the synthesis of Si_3N_4–TiN composites using the in situ reaction between Si_3N_4 and Ti powders.

Spark plasma sintering (SPS) has been developed for the fabrication of ceramics and metallic materials [14]. This process allows rapid sintering due to the direct heating of

* Corresponding author at: Department of Nano-structure and Advanced Materials, Graduate School of Science and Engineering, Kagoshima University, 1-21-40 Korimoto, Kagoshima 890-0065, Japan. Tel.: +81 99 2857704; fax: +81 99 2857704.
E-mail address: sueyoshi@mech.kagoshima-u.ac.jp (H. Sueyoshi).

0272-8842/$36.00
doi:10.1016/j.ceramint.2009.09.029

powder and dies by pulsed direct current electrification. This implies that the die also acts as a heating source and that the sample is heated from both outside and inside. Besides, an external electrical field setting up plays an important role in enhancing mass-transportation. A unique feature of SPS process is thus to enable reaction and consolidation to occur at comparatively lower temperature in a rapid manner.

In this paper, we report the preparation of electroconductive Si_3N_4–TiN composites from Si_3N_4 and Ti powders using planetary ball milling. Powder mixtures were consolidated by SPS and the influences of sintering temperature on microstructure, hardness and electrical resistivity of composites were investigated.

2. Experimental procedure

Starting materials were Si_3N_4 powder (Wako Co. Ltd.) containing 5 mass% Y_2O_3 and 2 mass% Al_2O_3 as sintering additives and Ti powder (Wako Co. Ltd.). The mean particle sizes of Si_3N_4 and Ti powders are 60 nm and 45 μm, respectively. The milling process was carried out in ethanol using high energy planetary ball mill (Pulverisette 6, Fritsch Co. Ltd.). Si_3N_4–30 mass% Ti powders were mixed in a pot together with Si_3N_4 ball (5 mm diameter). The powder to ball weight ratio was 1:20, milling speed was 200 rpm and milling time was 30 h. The slurry was dried in an oven at 80 °C for overnight, and the dried agglomerates were ground with a mortar and pestle to pass through a 200 mesh sieve to pulverize the aggregates.

The milled powders of 2 g were put into a graphite die with an inner diameter of 15 mm. A graphite sheet of 0.25 mm thickness was used to prevent powder/die and powder/punch reactions. The SPS processing (SPS-3.20 MK-4, Sumitomo Coal Co. Ltd.) was carried out in vacuum (10 Pa) by heating at a rate of 100 °C/min to the sintering temperature (1200–1600 °C) and holding for 10 min. The pressure applied was 40 MPa and temperature was measured by an infrared ray thermometer focused on the surface of the graphite die. During heating, the change in thickness of the specimen was measured by a dilatometer to monitor the densification behavior.

The density of the sintered compacts was measured by the Archimedes method (MD-300S, Alfa Mirage Co. Ltd.). The microstructure of the polished and plasma-etched (Tensec SP10, Horiba Co. Ltd.) specimen was examined using a scanning electron microscope (ESEM XL-30 Series, Philips Co. Ltd.) and an energy dispersive X-ray spectrometer (EDX) installed in the ESEM. The crystalline structure was examined by X-ray diffraction (XRD, X'Pert PRO MPD, PANalytical Co. Ltd.), which was performed with Cu Kα-ray at a scanning rate of 3°/min. Chemical states of atoms in the sintered compacts were investigated by X-ray photoelectron spectroscopy (XPS; ESCA-1000, Shimadzu Co. Ltd.) with Mg Kα irradiation (1.253 keV). The surfaces were removed by Ar^+ ion milling for 5 min, before the XPS analyses. The Vickers micro-hardness of the sintered compacts under a load of 9.807 N was measured using Vickers hardness tester (HMV, Shimadzu Co. Ltd.). The DC electrical resistivity was measured at room temperature on the polished surface of the specimen (2 mm × 3 mm × 14 mm) using a four-point probe method. The machinability of the sintered compacts was examined by EDM (Robocut α-OA, Fanuc Co. Ltd.) with 0.25 mm diameter of Cu wire at a feed speed of 0.2 mm/min.

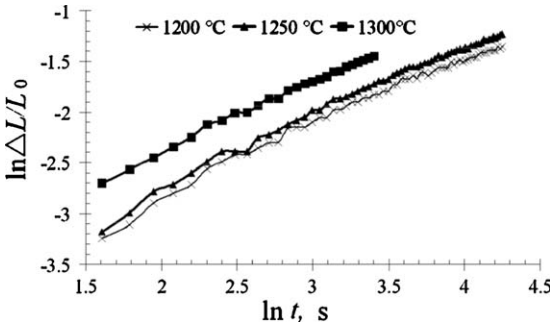

Fig. 1. Relationships between logarithmic shrinkage and logarithmic holding time for the initial stage of sintering.

3. Results

Fig. 1 shows the relationships between logarithmic shrinkage ($\ln \Delta L/L_o$) and logarithmic holding time ($\ln t$) for the initial stage of sintering. In SPS at temperature higher than 1350 °C, the densification process was completed at the initial stage of holding. Kingery et al. [15,16] proposed a relation between logarithmic shrinkage and logarithmic holding time based on a theoretical consideration during the initial stage of sintering. According to the relationships, liquid phase sintering dominated by the dissolution–reprecipitation mechanism, the slope $k = 0.5$ [15] and viscous flow, $k = 1$ [16]. The slopes shown in Fig. 1 were 0.668, 0.687 and 0.687 at 1200, 1250 and 1300 °C, respectively. Therefore, the dominant mechanism for SPS is a hybrid of dissolution–reprecipitation and viscous flow.

The resulting bulk density and Vickers hardness of the sintered compacts is graphically presented in Fig. 2. The density increased with increasing sintering temperature up to a maximum of 3.41 g/cm^3 at 1350 °C, but almost no changes (∼3.30 g/cm^3) could be seen as the temperature increased to 1600 °C. The hardness increased with increasing sintering temperature up to a maximum of 19.95 GPa at 1350 °C, then decreased progressively with increasing sintering temperature.

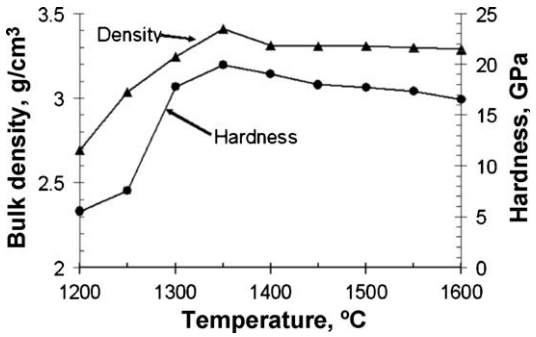

Fig. 2. Bulk density and Vickers hardness of sintered compacts vs. sintering temperature.

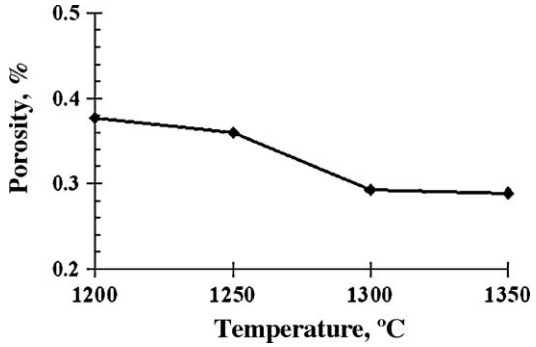

Fig. 3. Porosity of sintered compacts vs. sintering temperature.

This maximum hardness is significantly higher than that of composites prepared by Gao et al. [8]; maximum hardness of Si_3N_4–20 vol% TiN composites (14 GPa) were produced by HP at 1600 °C for 1 h under a compressive stress of 30 MPa. Fig. 3 shows the effect of sintering temperature on the porosity of sintered compacts. The decrease in porosity was observed in the case of SPS at higher temperatures. When sintered at temperatures higher than 1300 °C, the porosity of the sintered compacts reached only 0.3%. Thus SPS led to the high density and hardness and reduction in porosity of the sintered compacts. In SPS, densified compact was achieved at a lower sintered temperature compared with conventional sintering techniques such as HP. The sintering time required for SPS was less than that required for HP. SPS uses high pulsed current to generate spark plasma and Joule heating at the contact area between powder particles. This SPS characteristic could be the reason to produce a liquid phase at grain boundary at a lower temperature. These suggest that SPS is an efficient sintering process for fabricating Si_3N_4–TiN composites.

Fig. 4 shows back-scattered electron (BSE) images of cross-section of sintered compact prepared by SPS at 1250 °C. Sintered compact exhibited a microstructure with long shaped TiN (white area) in Si_3N_4 (black area) as shown in Fig. 4(a). The EDX analysis of circled part in Fig. 4(b) revealed that the area is composed of Ti, Si, N and O.

Fig. 5 shows XRD patterns of the starting powders, milled powder and sintered compacts prepared by SPS at different temperatures. α and β-Si_3N_4 peaks were present in the as-received Si_3N_4 powder. α and β-Si_3N_4 and Ti were detected in milled powder. XRD patterns showed that TiN present in all sintered compacts. This indicates that the stability of TiN in Si_3N_4 is well and there is no obvious reaction between each

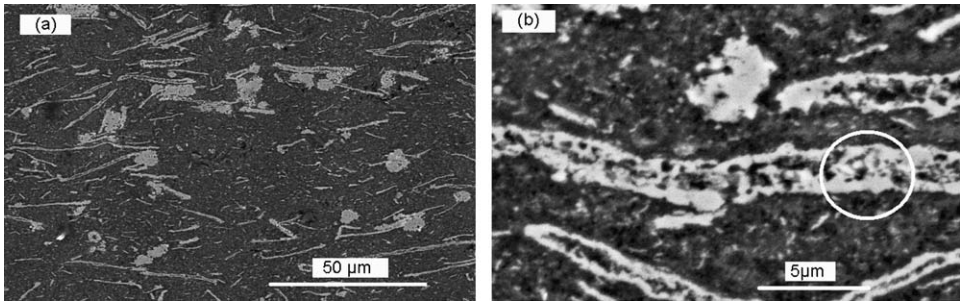

Fig. 4. BSE images of cross-section of sintered compact prepared by SPS at 1250 °C: (a) low magnification and (b) high magnification.

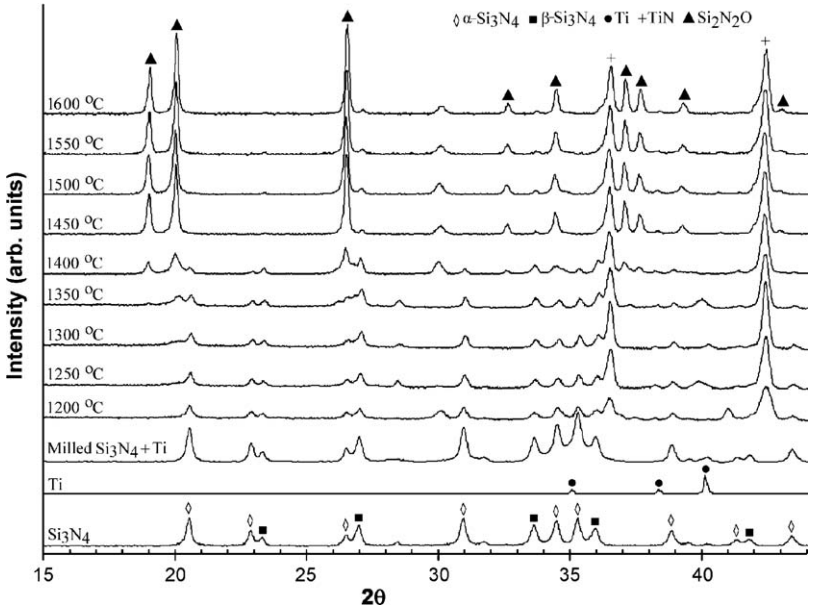

Fig. 5. XRD patterns of starting powders, milled powder and sintered compacts prepared by SPS at different temperatures.

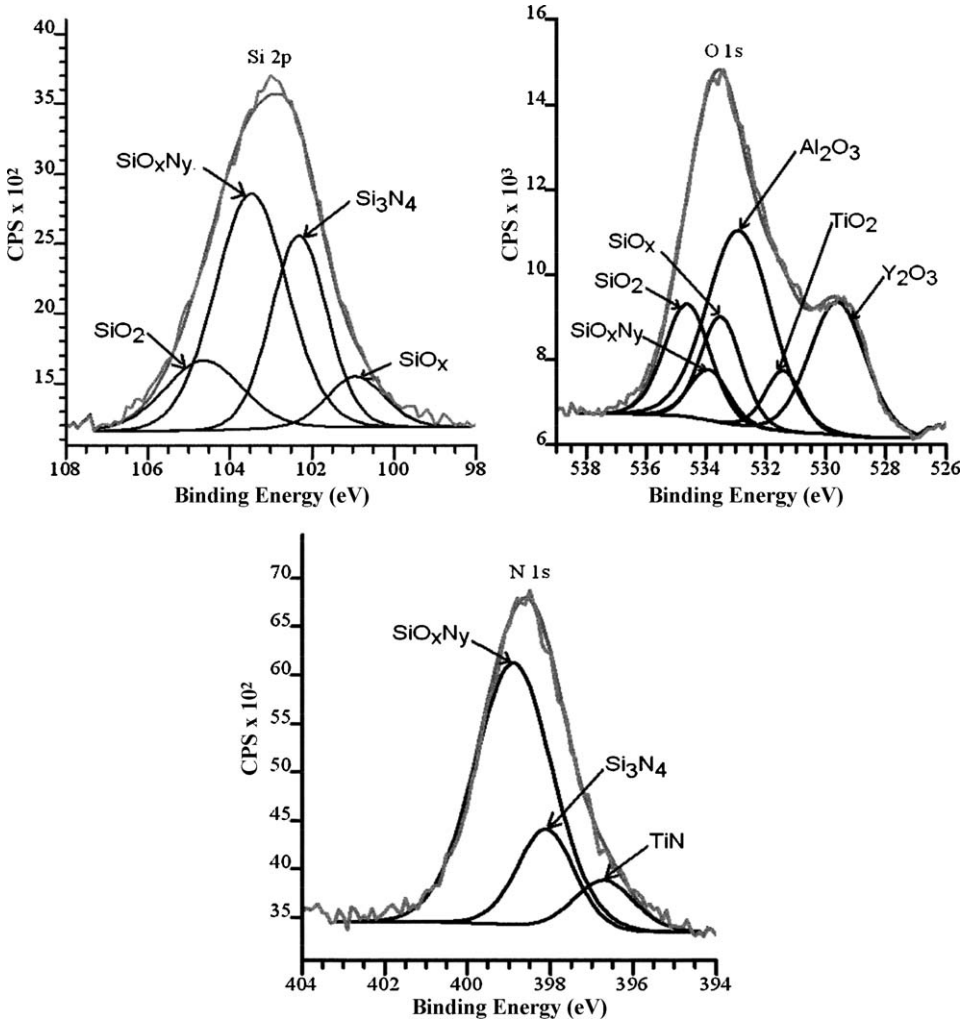

Fig. 6. Si 2p, O 1s and N 1s regions of XPS spectra of sintered compact prepared by SPS at 1300 °C.

other. The sintered compact prepared by SPS at 1200 °C had a small amount of TiN. However, the amount of TiN was similar when the sintering temperature was higher than 1250 °C. At 1200–1350 °C, the amount of α-Si_3N_4, decreased with increasing sintering temperature, while the amount of β-Si_3N_4 increased with increasing sintering temperature. At temperature higher than 1350 °C, Si_2N_2O peaks were clearly detected, while the intensities of α and β-Si_3N_4 peaks decreased. Si_2N_2O have a low density and hardness compared with Si_3N_4. The formation and growth of β-Si_3N_4 and TiN in addition to the densification of matrix by SPS also led to the increase in hardness and density of the composites from 1200 to 1350 °C. On the other hand, the decrease in density and hardness at higher sintering temperature can be attributed to the formation of Si_2N_2O having a low density and hardness compared with Si_3N_4.

XPS spectra of Si 2p, O 1s and N 1s electrons obtained from the sintered compact produced by SPS at 1300 °C are shown in Fig. 6. Table 1 shows the data for binding energy and FWHM from shifted peak in the carbon (C 1s) referenced peak at 285.7 eV and FWHM 1.4 eV. The XPS spectra for Si 2p revealed the presence of four peaks corresponding to SiO_x, Si_3N_4, SiO_xN_y and SiO_2. In the corresponding O 1s and N 1s spectra, SiO_xN_y was also observed. Another O 1s peaks correspond to oxygen in Y_2O_3 and Al_2O_3 which originate from the starting materials of Si_3N_4 as a sintering additive. The

Table 1
The data of XPS measurements for sintered compact prepared by SPS at 1300 °C.

Orbital	Position measured	Position shifted	FWHM	Functionality
Si 2p	100.9	100.2	1.64	SiO_x [17]
	102.3	101.6	1.6	Si_3N_4 [17]
	103.5	102.8	2.07	SiO_xN_y [18]
	104.6	103.9	2.2	SiO_2 [17]
O 1s	529.6	528.9	2.2	Y_2O_3 [17]
	531.2	530.5	3.1	TiO_2 [19]
	532.9	532.2	2.5	Al_2O_3 [17]
	533.9	533.2	1.56	SiO_xN_y [18]
	534.6	533.9	1.8	SiO_2 [17]
	533.5	532.8	1.62	SiO_x [17]
N 1s	396.7	396.0	1.71	TiN [20]
	398.1	397.4	1.61	Si_3N_4 [21]
	398.9	398.2	2.2	SiO_xN_y [18]

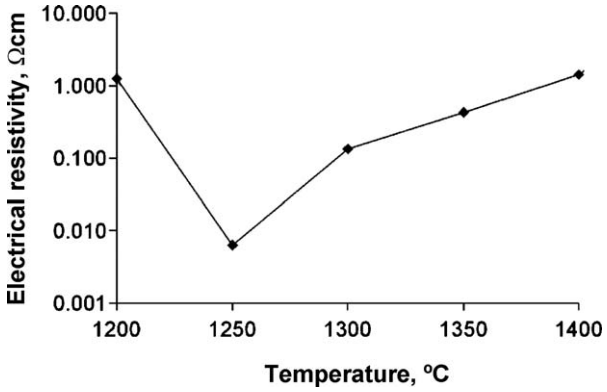

Fig. 7. Electrical resistivity of sintered compacts.

amount of TiO_2 may be small because TiO_2 peaks did not reveal in XRD pattern. The XPS spectrum of N 1s revealed the presence of three peaks corresponding to SiO_xN_y, Si_3N_4 and TiN.

Fig. 7 shows the electrical resistivity of sintered compacts prepared by SPS. The electrical resistivity decreased from 1.24 to 6.3×10^{-3} Ω cm as sintering temperature increased from 1200 to 1250 °C. When the sintering temperature exceeded 1250 °C, it increased with increasing sintering temperature. The sintered compact prepared by SPS at 1200 °C has many pores (Fig. 3) and the small amount of TiN (Fig. 5), resulting in high electrical resistivity. The sintered compact prepared by SPS at 1250 °C has a small amount of pore and the large amount of TiN, resulting in low electrical resistivity. Si_2N_2O has high electrical resistivity. The increases in electrical resistivity at temperature range of 1250–1400 °C are due to the increases in the amount of Si_2N_2O. The value of resistivity (6.3×10^{-3} to 1.42 Ω cm) of the sintered compacts prepared by SPS at 1250–1400 °C is small compared with that of Si_3N_4–TiN composites obtained by Gao et al. (2 Ω cm), which is produced by HP at 1650 °C for 1 h [8].

Fig. 8 showed the optical micrograph of sintered compacts prepared by SPS at 1200 and 1300 °C, followed by EDM. The sintered compact prepared by SPS at 1200 °C could not be machined by EDM, while the sintered compacts prepared by SPS at 1250–1350 °C could be easily machined by EDM. In this case, machinability decreased with the increase in sintering temperature. This behavior corresponds to the change in electrical resistivity. The sintered compacts prepared by SPS at 1400–1600 °C also could not be machined by EDM. This is because electrical resistivity is high. Thus, the sintered compact prepared by SPS at 1300 °C had high hardness (17.78 GPa) and density and a good machinability.

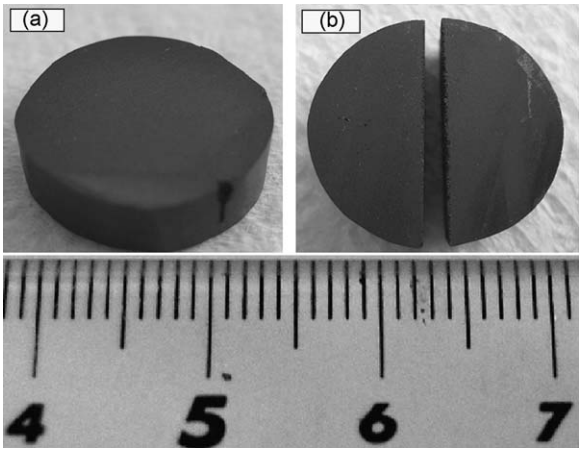

Fig. 8. Optical micrograph of sintered compacts prepared by SPS at (a) 1200 °C and (b) 1300 °C followed by EDM.

4. Discussion

From the thermodynamic point of view Ti has a great affinity for oxygen, according to the reaction:

$$Ti + O_2 \rightarrow TiO_2 \quad (1)$$

During milling, no oxidation occurs because it is conducted in ethanol. Oxidation may occur when milled powders are removed from milling pot, dried in an oven and compacted in the graphite mold for SPS. Oxidation is promoted by SPS because of residual oxygen present in the compact. TiO_2 formed on the surface of Ti powder reacts with Si_3N_4 to form TiN.

$$(1/3)Si_3N_4 + TiO_2 \rightarrow SiO_2 + TiN + (1/6)N_2 \quad (2)$$

On the other hand, residual Ti reacts with Si_3N_4 to form TiN.

$$(1/4)Si_3N_4 + Ti \rightarrow TiN + (3/4)Si \quad (3)$$

Besides reaction (2), the reaction of Si_3N_4 becomes consistent, leading to the formation of silicon oxynitride at higher temperature, according to reaction (4)

$$Si_3N_4 + SiO_2 + Ti + (1/2)N_2 \rightarrow TiN + Si_2N_2O \quad (4)$$

Reaction (4) involves the dissolution of Si_3N_4 into SiO_2 melt, which provides an easy transport medium for the reaction. Al_2O_3 and Y_2O_3 which added as a sintering additive usually lower the viscosity of the liquid phase and thereby lower the reaction temperature and enhance the transformation kinetics.

According to the calculation results (using HSC Chemistry 5 in Outokumpu Research) of thermochemical data by using the relationship between temperature and the standard Gibbs-free energy (ΔG°), reactions (1)–(4) are shown in Fig. 9. It can be seen that ΔG° of all reactions are negative in the experimental temperature range, indicating that reactions (1)–(4) can take place thermodynamically in this work. From Fig. 1, the sintering mechanisms for SPS are a hybrid of dissolution–reprecipitation and viscous flow. The reprecipitated β-Si_3N_4 is nodular. This nodular β-Si_3N_4 reacts with TiO_2 and Ti. The long shaped TiN (white area) in Fig. 4(a) is due to the formation of homogeneous TiN grains along the nodular β-Si_3N_4. Furthermore, the presence of Ti, Si, N and O at circled part in Fig. 4(b) is based on reaction (4), that is, the formation of Si_2N_2O and TiN. As sintering temperature becomes high, oxidation of Ti is promoted, resulting in the increase of the amount of Si_2N_2O and resultant high electrical resistivity as shown in Fig. 7.

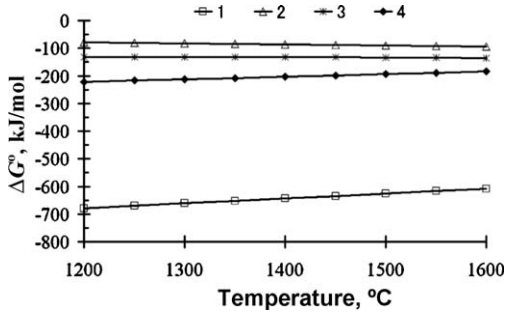

Fig. 9. Relation between standard Gibbs-free energy and temperature.

5. Conclusions

Electroconductive Si_3N_4–TiN composites were achieved by SPS at 1250–1350 °C using 70 mass% Si_3N_4 (with additives 5 mass% Y_2O_3 and 2 mass% Al_2O_3) and 30 mass% Ti powders as raw materials. The sintering mechanism for SPS was a hybrid of dissolution–reprecipitation and viscous flow. The hardness and electrical resistivity depended upon sintering temperature. The hardness increased with increasing sintering temperature up to a maximum at 1350 °C, then decreased progressively with increasing temperature. The electrical resistivity decreased with increasing sintering temperature up to a minimum at 1250 °C, then increased with increasing sintering temperature. Composites sintered at 1250–1350 °C could be easily machined by EDM. In summary, composite prepared by SPS at 1300 °C showed a high hardness (17.78 GPa) and a good machinability.

Acknowledgements

The authors would like to thank sincerely Mr. Yosihisa Oozono (from Division of Instrumental Analysis, Frontier Science Research Center, Kagoshima University) for his assistance in conducting XPS analyses and appreciate the Hitachi Scholarship Foundation (Tokyo) for the scholarship.

References

[1] F.L. Riley, Silicon, nitride and related materials, J. Am. Ceram. Soc. 83 (2) (2000) 245–265.
[2] G. Petzow, M. Herrmann, Silicon nitride ceramics, Struct. Bond. 102 (2002) 147–167.
[3] C.Y. Chu, J.P. Singh, J.L. Routbort, High-temperature failure mechanisms of hot-pressed Si_3N_4 and Si_3N_4/Si_3N_4 whiskers-reinforced composites, J. Am Ceram. Soc. 76 (5) (1993) 1349–1353.
[4] H.H.K. Xu, C.P. Ostertag, L.M. Braun, Effects of fiber volume fraction on mechanical properties of SiC–fiber/Si_3N_4 matrix composites, J. Am. Ceram. Soc. 77 (7) (1994) 1897–1900.
[5] D.W. Shin, H. Tanaka, Low temperature processing of ceramic woven fabric/ceramic matrix composites, J. Am. Ceram. Soc. 77 (1) (1994) 97–104.
[6] T. Nagaoka, M. Yasuoka, K. Hirao, S. Kanzaki, Effects of TiN particle size on mechanical properties of Si_3N_4/TiN particulate composites, J. Ceram. Soc. Jpn. 100 (1992) 617.
[7] K. Kamiya, T. Yoko, Nitridation of TiO_2 fibres prepared by the sol–gel method, J. Mater. Sci. 22 (1987) 937.
[8] L. Gao, J. Li, T. Kusunose, K. Niihara, Preparation and properties of TiN–Si_3N_4 composites, J. Eur. Ceram. Soc. 24 (2004) 381–386.
[9] M. Yoshimura, O. Komura, A. Yamakawa, Microstructural and tribological properties of nano-sized Si_3N_4, Scr. Mater. 44 (2001) 1517–1521.
[10] K. Kawano, J. Takahashi, S. Shimada, Highly electroconductives TiN/Si_3N_4 composites fabricated by spark plasma sintering of Si_3N_4 particles with a nano size TiN coating, J. Mater. Chem. 12 (2002) 361–365.
[11] Z. Guo, et al., Microstructure and electrical properties of Si_3N_4–TiN composites sintered by hot pressing and spark plasma sintering, Ceram. Int. 33 (7) (2007) 1223–1229.
[12] T. Hirai, S. Hayashi, Preparation & some properties of chemically vapour deposited Si_3N_4–TiN composite, J. Mater. Sci. 17 (1982) 1320.
[13] N. Ahmad, H. Sueyoshi, K. Obara, S. Sameshima, Si_3N_4–TiN composites consolidated by spark plasma sintering, in: Proceedings of 7th International Conference on Composites Science and Technology, 2009, pp. 1–6.
[14] M. Tokita, Mechanism of spark plasma sintering, J. Powder Technol. Japan 30 (11) (1993) 790–804.
[15] W.D. Kingery, Densification during in the presence of a liquid phase. I. Theory, J. Appl. Phys. 30 (1959) 301–306.
[16] W.D. Kingery, M. Berg, Study of the initial stage of sintering solids by viscous flow, evaporation–condensation and self-diffusion, Appl. Phys. 26 (1956) 1205–1212.
[17] C.D. Wagner, A.V. Naumkin, A. Kraut-Vass, J.W. Allison, C.J. Powell, J.R. Rumble, Jr., NIST X-Ray Photoelectron Spectroscopy Database, NIST Standard Reference Database 20, 2007, Version 3.5 (Web Version; http://srdata.nist.gov/xps/Default.aspx).
[18] R. Mroezynski, et al., Comparison of composition of ultra-thin silicon oxynitride layers fabricated by PECVD and ultrashallow of plasma ion implantation, J. Telecommun. Inform. Technol. 3 (2007) 20–24.
[19] A. Vesel, M. Mozetic, J. Kovac, A. Zalar, XPS study of the deposited Ti layer in a magnetron-type sputter ion pump, Appl. Surf. Sci. 253 (2006) 2941–2946.
[20] N. Jiang, H.J. Zhang, S.N. Bao, Y.G. Shen, Z.F. Zhou, XPS study for reactively sputtered nitride thin films deposited under different substrate bias, Phys. B 352 (2004) 118–126.
[21] T.N. Taylor, D.P. Butt, Auger parameter determination of bonding states on thinly oxidized silicon nitride, in: Surface Analysis 97 and 33rd Annual Symposium of the NM Chapter on the AVS in Albuquerque, NM, (1997), pp. 1–29.